Dropwise Condensation Underneath Chemically Textured Surfaces: Simulation and Experiments

Basant Singh Sikarwar

Nirmal Kumar Battoo

Sameer Khandekar[1]
e-mail: samkhan@iitk.ac.in

K. Muralidhar

Department of Mechanical Engineering,
Indian Institute of Technology Kanpur,
Kanpur 208016, India

Experimental observations of dropwise condensation of water vapor on a chemically textured surface of glass and its detailed computer simulation are presented. Experiments are focused on the pendant mode of dropwise condensation on the underside of horizontal and inclined glass substrates. Chemical texturing of glass is achieved by silanation using octyl-decyl-tri-chloro-silane ($C_{18}H_{37}C_{13}Si$) in a chemical vapor deposition process. The mathematical model is built in such a way that it captures all the major physical processes taking place during condensation. These include growth due to direct condensation, droplet coalescence, sliding, fall-off, and renucleation of droplets. The effects arising from lyophobicity, namely, the contact angle variation and its hysteresis, inclination of the substrate, and saturation temperature at which the condensation is carried out, have been incorporated. The importance of higher order effects neglected in the simulation is discussed. The results of model simulation are compared with the experimental data. After validation, a parametric study is carried out for cases not covered by the experimental regime, i.e., various fluids, substrate inclination angle, saturation temperature, and contact angle hysteresis. Major conclusions arrived at in the study are the following: The area of droplet coverage decreases with an increase in both static contact angle of the droplet and substrate inclination. As the substrate inclination increases, the time instant of commencement of sliding of the droplet is advanced. The critical angle of inclination required for the inception of droplet sliding varies inversely with the droplet volume. For a given static contact angle, the fall-off time of the droplet from the substrate is a linear function of the saturation temperature. For a given fluid, the drop size distribution is well represented by a power law. Average heat transfer coefficient is satisfactorily predicted by the developed model. [DOI: 10.1115/1.4002396]

Keywords: dropwise condensation, chemical texturing, pendant droplets, modeling and simulation, imaging

1 Introduction

It is well known that the heat transfer coefficient during dropwise condensation is several times larger than other modes of condensation. Dropwise condensation could be promoted by introducing a nonwetting chemical into the vapor, by special physical treatment of the condensation surface/substrate, or by chemical coating of the solid substrate with a low surface-energy substance [1–3]. These techniques have been known for many years; the last technique holds considerable promise and has been an active area of research. Marto et al. [4] tested several polymer coatings, gold and silver, for sustaining dropwise condensation of steam and reported the heat transfer coefficients in dropwise condensation as high as six times when compared with filmwise condensation. Zhao et al. [5] reported that the heat transfer coefficients of dropwise condensation on Langmuir–Blodgett treated surfaces are more than 30 times higher than that of filmwise condensation on bare surfaces. Vemuri et al. [6] experimentally investigated the effects of various chemical coatings and their long term durability on the dropwise mode of heat transfer. They reported a decrease in heat transfer coefficient with the elapsed condensation time, suggesting possible leaching of the chemical coating. Rausch et al. [7] reported that the heat transfer coefficient on an ion-implantation surface is more than five times that of filmwise condensation. In recent years, with the advent of newer coating/manufacturing and nanoscale fabrication techniques, promoting long term sustainability of dropwise condensation by chemical coating now holds considerable prospect for enhancing heat transfer in a variety of industries [2,6,8]. An example of enhanced performance of compact steam condensers having chemically coated flow passages of only a few millimeter width is demonstrated by Majumdar and Mezic [9].

Apart from the dropwise condensation process for heat transfer applications, the formation of distinct drops on horizontal/inclined lyophobic surfaces and their subsequent dynamics is also of considerable interest in many other industrial and engineering applications such as microfluidics, lab-on-chip device, ink jet printing systems, spraying of insecticide on crops, and several biochemical processes [10]. The understanding of the dynamics of the droplet ensemble also gains importance if droplet-substrate interaction leads to physico-chemical leaching of the substrate, for example, during (i) estimation of the life cycle of a heat exchanger textured by promoter layers and (ii) estimation of substrate life on which heavy liquid metals are being deposited under closed vacuum conditions [11].

The phenomenon of droplet formation and the exact mechanism of enhancement of heat transfer by condensation on chemically textured surfaces have been a matter of debate and discussion. It depends not only on the thermophysical properties of the fluid

[1]Corresponding author.

Contributed by the Heat Transfer Division of ASME for publication in the JOURNAL OF HEAT TRANSFER. Manuscript received April 29, 2010; final manuscript received July 23, 2010; published online November 3, 2010. Assoc. Editor: Giulio Lorenzini.

Downloaded 08 Nov 2010 to 202.3.77.11. Redistribution subject to ASME license or copyright; see http://www.asme.org/terms/Terms_Use.cfm

getting condensed, but also on the physico-chemical properties of the substrate, time scales involved, process control parameters, external body forces other than gravity (such as electro-wetting), orientation and texture of the cold substrate, applicable subcooling, etc. Leach et al. [12] reported that the contribution of small drops to the overall heat transfer coefficient exceeds that of the largest drops by a factor of 15. McCormick and Baer [13] reported that the droplet nucleation, growth patterns, and subsequent droplet dynamics have important practical consequences on high heat transfer rates. Experimental determination of the heat transfer coefficient is also a challenging task because of the many intricacies involved in the process. Mainly, the driving temperature difference is very small in dropwise condensation, essentially resulting in a very high heat transfer coefficient. Second, required spatio-temporal resolutions are also quite demanding, as recently demonstrated by Bansal et al. [14], who have experimentally determined the local wall heat transfer coefficient below a condensing single-droplet and multidroplet pendant system by liquid crystal thermography. They reported the variation in local heat flux at the base of the droplet as a function of its diameter (similar work on single-droplet and multidroplet systems evaporating on a heated surface in the context of spray cooling has been shown by Tartarini et al. [15] using high resolution infrared thermography). Heat transfer rates are also affected by sessile/pendant mode and global orientation of the substrate. On an inclined substrate, continuous sweeping of critically sized droplets and renewal of drop growth cycle is responsible for the higher heat transfer coefficient associated with dropwise condensation, as summarized by Leipertz and Fröba [2]. Briscoe and Galvin [16] and Lawal and Brown [17] experimentally compared the performance of sessile and pendant droplets and attributed the instability of the pendant mode for its better heat transfer coefficient.

Modeling of the dropwise condensation process based on nucleation hypothesis has been attempted by various investigators. Glicksman and Hunt [18] simulated the dropwise condensation cycle in a number of stages, covering the equilibrium drop size to the departing drop size, to achieve a large nucleation site density. The initial stage consisted of a nucleation site density of 10^8 m^{-2} by taking 1000 sites on a surface of size 33×33 μm^2. The area of the second stage was increased ten times, and the droplets from the first stage were redistributed on this surface. In this way, the simulation was repeated until the departure droplet size was reached. Thus, a high nucleation site density was achieved, but an artificial redistribution between two consecutive stages destroyed the natural distribution of the drops. Wu and Maa [19] and Maa [20] used the population balance method to find the drop size distribution of small drops, which grow mainly by direct condensation. They estimated the heat transfer coefficient by considering only the conduction resistance through the drop. Abu-Orabi [21] incorporated the resistance due to heat conduction through the promoting layer; curvature resistance was also included. Rose and Glicksman [22] proposed a universal form of the distribution function for large drops, which grow primarily by coalescence with smaller drops, though smaller drops themselves mainly grow by direct condensation. Gose et al. [23] carried out computer simulation on a 100×100 grid with 200 randomly distributed nucleation sites. Burnside and Hadi [24] simulated dropwise condensation of steam from an equilibrium droplet to a detectable size on 240×240 μm^2 surface with 60,000 randomly spaced nucleation sites. Later, Vemuri and Kim [25] modeled dropwise condensation for hemispherical drops, which mainly grow by direct condensation, by the population balance method. The primary resistances to heat transfer, such as conduction through the drop and vapor-liquid interface resistance, were considered in developing the model. The derivation of a steady state distribution for small drops within the size range of negligible coalescence was based on the conservation of the number of drops with no accumulation. Contact angle other than 90 deg was not considered in this model. Leach et al. [12] experimentally observed drop growth kinetics: The smallest drops grow principally by the accretion of liquid molecules diffusing along the substrate surface, while drops larger than about 50 μm in diameter grow principally by the accretion of condensing vapor directly onto the drop surface. Their model incorporated these growth mechanisms. They also reported the effect of contact angles, degree of subcooling, and inclination of a substrate on nucleation site densities onto a hydrophobic polymer film and a silanized glass surface for sessile droplets.

A complete simulation of dropwise condensation from the equilibrium droplet size to the departing droplet size, accounting for the effect of saturation temperature, contact angle and its hysteresis, and the inclination of the substrate along with its experimental validation, has not been explicitly reported. Against this background, the present study aims at (a) experimentally observing dropwise condensation on a chemically textured surface and (b) simulating the entire spatio-temporal process of dropwise condensation. The methodology adopted for the experimental study is

(i) recording high quality video images at sufficiently high speeds to capture the complete cycle of dropwise condensation, under controlled conditions, on the underside (pendant mode) of chemically textured horizontal and inclined surfaces. Silanes, which are known promoters of hydrophobicity, are used for coating the glass substrate; the corresponding static contact angles have been determined under laboratory conditions.
(ii) digital processing of the video data obtained in step (i) above to extract relevant spatio-temporal quantities of interest such as drop size distribution, area of coverage, droplet merger dynamics, coalescences, and fall-off and slide-off times.

The quantitative experimental data thus obtained, along with the observed qualitative behavior of dropwise condensation, are used for comparison with the developed simulation model. After code validation, parametric studies of dropwise condensation have been done incorporating the numerical code. While the broad outline of the model has been taken from Ref. [3], we have now substantially enriched its originally proposed simplistic approach, not only in the details of the relevant droplet force fields under any substrate inclination but also on the generic extent of the applicability of the model. The simulation of the process proceeds from the equilibrium droplet size to the departing droplet size underneath a horizontal and an inclined substrate, respectively. The extended transient model incorporates the effect of contact angle and its hysteresis and substrate inclination; it accounts for continuous droplet fall-off/slide-off, droplet coalescence and merger dynamics, and renucleation of droplets; thus, all the major physical phenomena seen in experiments have been incorporated in the present model.

Section 2 of the paper describes the design details of the experiment setup and its methodology. Section 3 describes the mathematical model in detail, including the assumptions involved. Section 4 describes the results obtained from the simulation and their comparison with the experiments. Finally, major conclusions of the present study are reported in Sec. 5.

2 Experimental Setup and Methodology

The experimental apparatus was designed to study dropwise condensation under controlled conditions on the underside of a cold substrate and is schematically shown in Fig. 1. The setup primarily consisted of the main cylindrical stainless steel vacuum chamber (better than 10^{-6} mbar abs.) of 180 mm inner diameter and 120 mm length (Figs. 1(*a*) and 1(*b*)). It was closed from the two ends by specially designed flanges. The lower flange was fitted with a $\lambda/4$ optical viewing window (view A; typical photographs of condensing droplets are shown in Fig. 1(*c*)). In addition, it also had an annular space around this viewing window wherein the working fluid inventory (distilled and de-ionized water) was

Downloaded 08 Nov 2010 to 202.3.77.11. Redistribution subject to ASME license or copyright; see http://www.asme.org/terms/Terms_Use.cfm

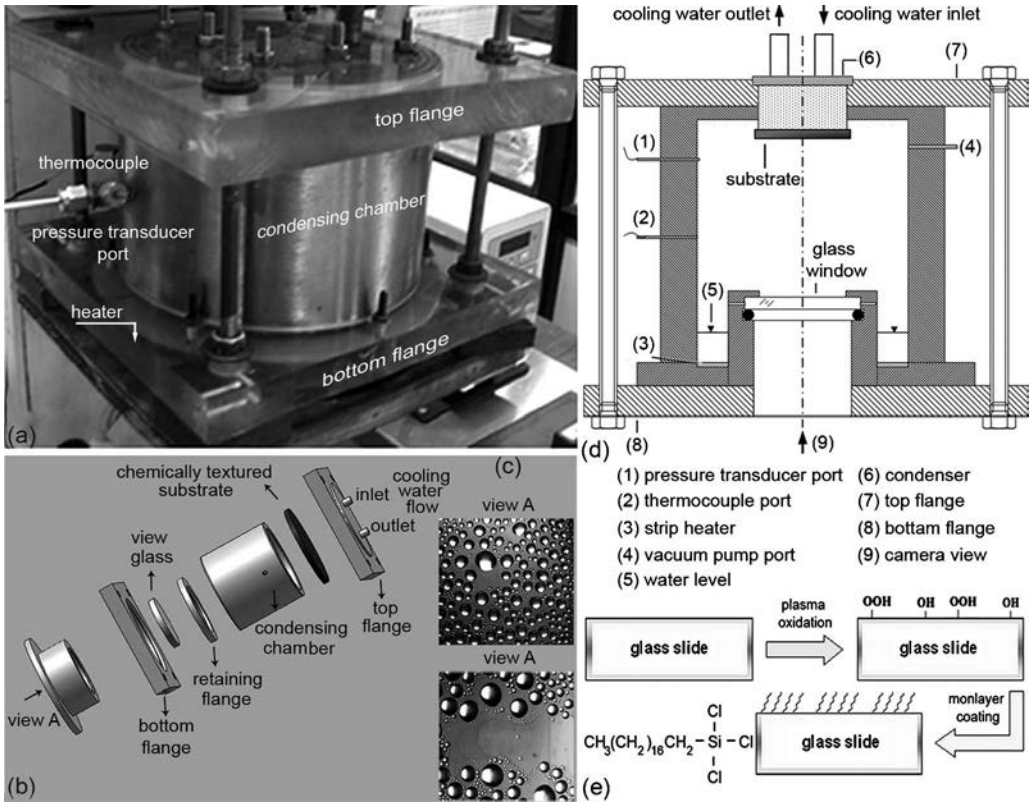

Fig. 1 Details of the experimental setup to study dropwise condensation under controlled conditions underneath a substrate. (*a*) Photograph shows the details of the main condensing chamber; (*b*) exploded view of the condensing chamber showing all the components. (*c*) Typical images of the condensing droplets at two different times, as captured from view A. (*d*) Cross-sectional view of condensing chamber. (*e*) Schematic diagram explaining the chemical vapor deposition process.

stored. A circular, 1.5 mm thick mica strip heater (o.d.=70 mm, i.d.=40 mm) was attached outside this annular space to give the necessary heat input, as shown in the cut section of the experimental setup in Fig. 1(*d*). The upper end of the main vacuum chamber was closed with a polycarbonate square flange with an inbuilt cavity wherein cold water was circulated to maintain constant temperature boundary conditions. The condenser capacity was at least 20 times that of the expected heat transfer rate. The chemically coated glass substrate (methodology of substrate preparation is explained in the next section) of 100×100 mm^2 was integrated on the upper flange, as shown. Connections for evacuation, pressure transducer, and temperature sensors were provided on the main condensing chamber wall. The temperature of the condensing vapor was measured with one K-type thermocouple (Omega®, 0.5 mm diameter) of accuracy of ±0.2°C after calibration. It was placed centrally in the chamber at a distance of 25 mm from its side wall. The condensing chamber pressure was measured by an absolute pressure transducer (Honeywell, accuracy 0.1% FS, NIST traceable calibration, range of 0–1.2 bars). Online data acquisition was carried out with 16 bit PCI-4351 card (National Instruments®). The entire assembly could be tilted to any desired inclination at 0–25 deg. A color charge coupled device (CCD) video camera (Basler® A202KC with 1024×1024 pixels at 100 fps) was used to capture the images of the drops forming on the underside of the chemically textured substrate (view A, Fig. 1(*b*)). Size scales were calibrated by imaging a grid with known periodicity. Diffused white light source symmetrically placed around the camera was directed on the substrate from the optical window on the bottom flange so as to maintain a near parallel and symmetric beam on the droplets, ensuring a proper contrast level for subsequent edge detection.

Dropwise condensation was achieved at the desired saturation pressure by controlling the coolant temperature and the heat throughput. Once a quasi-steady state was reached, the correspondence between the saturation pressure and the condensing vapor chamber temperature was continuously monitored. The high quality video images recorded were digitally processed (using IMAGE J® software) to get the relevant parameters of interest, i.e., area of coverage, droplet size distribution, fall-off/slide-off, coalescence/merger events, etc. The primary steps in finding the area of coverage were (a) digital image acquisition, (b) contrast thresholding and binning to reduce pixel noise, (c) droplet detection with geometry attributes, (d) measurement of total digitized pixel area covered by the droplets, and (e) finding the area of coverage by dividing the total pixel area of all the droplets by the total area of the acquired image. Droplets below a diameter of around 0.1 mm could not be resolved with the imaging hardware used. The image processing software is first tested against benchmark images before applying it on actual experimental images.

Surface Preparation (Chemical Texturing). The substrate preparation involved coating the glass surface using chemical vapor deposition (CVD) of silane molecules. The chemical vapor deposition setup consisted of a vacuum pump (rotary vane rougher pump coupled with diffusion pump, ultimate vacuum level $\sim10^{-5}$ mbar), a plasma oxidizer (with a rf generator having power levels of 6–18 W and frequencies of 8–12 MHz), and a desiccator. Inside the reactor, which was maintained at low vacuum pressure, the high frequency oscillating electromagnetic field ionized the silane molecules forming plasma. This interacted with the glass substrate by the following: (i) Removing organic contamination from its surface. The high energy plasma particles

Downloaded 08 Nov 2010 to 202.3.77.11. Redistribution subject to ASME license or copyright; see http://www.asme.org/terms/Terms_Use.cfm

combine with the contaminant to form carbon dioxide (CO_2) or methane (CH_4), and (ii) modifying the physico-chemical characteristics of surfaces by adsorption or chemisorption, etc. The silanation process is explained schematically in Fig. 1(*e*). Octyldecyl-trichloro-silane ($C_{18}H_{37}C_{13}Si$ supplied by M/s Sigma Aldrich®) was used as the coating material on the glass substrate. Before keeping the substrate for 30 min inside the CVD reactor, the substrate was cleaned by dipping it in a pirani solution (sulfuric acid and hydrogen peroxide in the ratio 3:1 by volume) for 2 h, thereafter washing it with distilled water and drying it in nitrogen. Nascent oxygen released when sulfuric acid reacts with hydrogen peroxide cleans the surface. The silane molecules attached themselves to the plasma cleaned glass plate, which was kept inside the CVD chamber, by a self-assembled monolayer process. After preparing the surface, the static, advancing, and receding contact angles of a pendant water drop for horizontal and inclined substrates were measured by a goniometer that had a special attachment for inclining the substrate.

3 Model Description

The simulation presented in this work is based on the postulate that droplet embryos form and grow at nucleation sites, while the portion of the surface between the growing droplets remains dry [26,27].[1] The nucleation sites are randomly distributed on the substrate. According to the Clausis–Claperyon equation, the size of the initial thermodynamically stable drop formed at a nucleus is of the order of magnitude of a few nanometers for the usual heat transfer fluids. Therefore, from an engineering standpoint, it is difficult to experimentally capture the initial nucleation density on freshly exposed surfaces. This necessitates the use of theoretical models for estimating the number of initial nucleation sites, for example, the proposal of Rose [28] and Mu et al. [29]. Leach et al. [12] reported that the initial drop nucleation density is a function of the degree of subcooling $\Delta T_{sat}=T_{sat}-T_w$ but is a weak function of the physico-chemical properties (resultant contact angle) of the cold substrate. Following the literature on the initial nucleation density and in view of the ensuing temperature difference for the range of interest, the nucleation density is assumed to be 10^9 m^{-2} in the present model. Initially, all the sites are occupied by the droplet of the smallest radius as determined from thermodynamic considerations. These droplets are allowed to grow by direct condensation followed by subsequent coalescence until, depending on the substrate inclination, the droplet attains critical size for either fall-off or slide-off. The simulation is confined to condensation underneath cold substrates with pendant drops.

3.1 Condensation Underneath a Horizontal Substrate. A pendant drop underneath a flat horizontal substrate is shown in Fig. 2(*a*). The drop is considered as a portion of a sphere of radius r making a contact angle θ. From the geometry, the drop volume V, area of liquid-vapor interface A_{lv}, and area of solid-liquid interface A_{sl} are given by

$$V=\frac{\pi r^3}{3}(2-3\cos\theta+\cos^3\theta) \tag{1}$$

$$A_{lv}=2\pi r^2(1-\cos\theta) \tag{2}$$

$$A_{sl}=2\pi r^2(1-\cos^2\theta) \tag{3}$$

For a specified wall subcooling (T_s-T_w), the smallest stable droplet size possible can be found form thermodynamic considerations as [3]

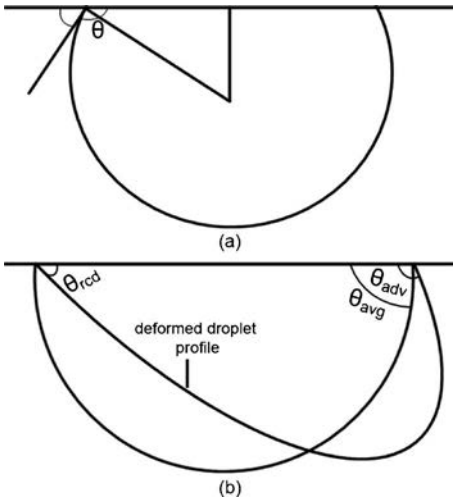

Fig. 2 (*a*) Schematic drawing of a pendant drop underneath a horizontal substrate with contact angle θ. (*b*) Drawing of a deformed drop with unequal advancing and receding angles, and its equivalent spherically approximated profile.

$$r_{min}=\frac{2\sigma\cdot\nu_l\cdot T_w}{h_{lv}[T_{sat}-T_w]} \tag{4}$$

Although the arguments leading to this equation do not include the substrate surface energy, Leach et al. [12] showed that such effects are of higher order and can be neglected for engineering calculations on the microscale. As droplets grow in size, the meso-/macroscale droplet dynamics cannot neglect the bulk contact angle ensuing from the surface energy of the substrate. The maximum drop diameter is calculated from balancing the surface tension with the weight of the drop and is derived as[2]

$$r_{max}=\sqrt{\left(\frac{6\sin^2\theta}{2-3\cos\theta+\cos^3\theta}\right)\cdot\left(\frac{\sigma}{g\cdot(\rho_l-\rho_v)}\right)} \tag{5}$$

The temperature drop due to various resistances to heat transfer is calculated as follows:

(i) Conduction resistance: The drop in temperature due to conduction heat transfer is determined as

$$\Delta T_{cond}=\frac{q\cdot r}{4\pi\cdot r^2\cdot k_c(1-\cos\theta)} \tag{6}$$

(ii) The temperature drop due to interfacial heat transfer is

$$\Delta T_{int}=\frac{q}{2\pi\cdot r^2\cdot h_i(1-\cos\theta)} \tag{7}$$

(iii) Curvature resistance: This resistance includes the loss of driving temperature potential due to the droplet interface curvature and is given by [3]

$$\Delta T_{curv}=\frac{2\nu_l\cdot\sigma\cdot T_w}{h_{lv}\cdot r}=\frac{(T_{sat}-T_w)r_{min}}{r} \tag{8}$$

The interfacial heat transfer coefficient is given by

[1]Another postulation suggests that condensation initially occurs in a filmwise manner, forming an extremely thin film on the solid surface. As condensation continues in time, this film ruptures forming distinct droplets which subsequently grow. This mechanism is not followed in the present work.

[2]Eq. (5) can be interpreted as modified Bond number criterion, applicable for a pendant droplet which takes into account the effect of contact angle in the force balance. In case of a horizontal substrate, there is no contact angle hysteresis. The usual definition of Bond number is given by, $Bo=(2\cdot r)(\sqrt{(g(\rho_l-\rho_v))/\sigma})$

Downloaded 08 Nov 2010 to 202.3.77.11. Redistribution subject to ASME license or copyright; see http://www.asme.org/terms/Terms_Use.cfm

$$h_i = \left(\frac{2\hat{\sigma}}{2-\hat{\sigma}}\right)\cdot\left(\frac{h_{lv}^2}{T_s \nu_{lv}}\right)\cdot\left(\frac{\bar{M}}{2\pi \bar{R} T_{sat}}\right)^{1/2} \quad (9)$$

Here, h_i is the interfacial heat transfer coefficient and k_c is the condensate thermal conductivity.

The temperature drop will balance the total available subcooling, and so,

$$\Delta T_t = \Delta T_{cond} + \Delta T_{int} + \Delta T_{curv} = \Delta T_{sat} \quad (10)$$

The heat flux through a single droplet is derived as

$$q = (\pi r^2 \rho_l h_{lv})\cdot(2 - 3\cos\theta + \cos^3\theta)\cdot\left(\frac{dr}{dt}\right) \quad (11)$$

From the above equation, the rate of growth of individual droplets is as follows:

$$\frac{dr}{dt} = \left(\frac{4\Delta T_t}{\rho_l \cdot h_{lv}}\right)\cdot\left[\frac{\left(1-\frac{r_{min}}{r}\right)}{\left(\frac{2}{h_i}+\frac{r}{k_c}\right)}\right]\cdot\left(\frac{(1-\cos\theta)}{(2-3\cos\theta+\cos^3\theta)}\right) \quad (12)$$

Equation (12) has been integrated to determine the growth of the droplet due to direct condensation. Along with the direct condensation growth loop in the simulator, a parallel coalescence loop is also monitored at each time step. The time for coalescence is taken to be much smaller than the other time scales of the condensation process. Hence, as soon as two droplets contact each other (or three droplets or, very rarely, four droplets contact each other simultaneously), they are substituted with an equivalent single droplet with a conserved volume, located at the weighted center of mass of the individual coalescing droplets.[3] At each time step, the nucleation sites, which are covered by drops, are checked and flagged as hidden sites. In this manner, the randomly distributed droplets are allowed to grow to a stage where their weight exceeds the retention surface force, yielding the critical Bond number criterion given by Eq. (5). At this juncture, droplets fall off. The drop is then removed, and all hidden nucleation sites underneath the drop become active and instantaneously supplied with thermodynamically stable droplets of minimum radius. It is to be noted that the simulation needs to track multiple generations of the droplets—nucleating, growing by direct condensation and by coalescence, and some falling-off when the virgin surface thus exposed is renucleated. The cycle thus begins again and is repeated for a long duration until a dynamic quasi-steady state is reached.

3.2 Condensation Underneath an Inclined Substrate. Inclining the substrate causes imbalance in the forces and results in drop deformation to achieve necessary static balance. As the droplet grows in size, the gravity force component parallel to the substrate exceeds the force component due to surface tension and will eventually cause the droplet to slide underneath the substrate. As droplets slide, they encounter other growing droplets on their path. This process results in a very rapid mass accumulation, as the sliding droplet sweeps away a large population of drops located ahead of it. The critical drop diameter at which sliding commences depends not only on the thermophysical properties of the liquid but also on the contact angle hysteresis and physicochemical properties of the substrate. Moreover, under dynamic conditions of dropwise condensation, the applicability of static force balances is questionable due to the presence of capillary waves, distortion in local equilibrium droplet shapes, droplet pinning, variation in dynamic contact angle due to inertia effects, local sudden acceleration, and three dimensional flow structures inside the droplets [33–35]. Therefore, there is a considerable debate in the literature on the applicability of static conditions on the real-time condensation process [36]. The bulk composite effect of these real-time dynamic situations and local contact line perturbations is usually manifested in the form of varying hysteresis of advancing and receding angles. Therefore, the static force balance conditions are assumed to be representative of the dynamic situation as absolute contact angles and hysteresis are accounted for.

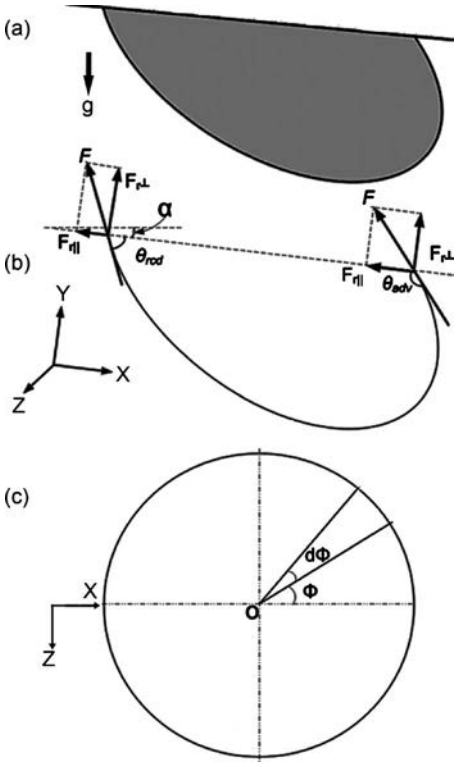

Fig. 3 (*a*) A deformed pendant drop underneath an inclined substrate. (*b*) Free body diagram of a static drop underneath an inclined surface. (*c*) Base of droplet on the substrate taken as a circle.

The contact angle hysteresis, namely, the variation in the advancing to the receding contact angle, is taken to vary linearly along the contact line (refer Fig. 3). While alternative strategies are available [37,38], this approach has been adopted earlier [39]. The variation in contact angle, with respect to azimuthal angle along the contact line, is formulated as

$$\theta = \theta_{adv} + \frac{(\pi - \theta_{rcd} - \theta_{adv})}{\pi}\phi \quad (13)$$

Figure 3(*a*) shows a deformed pendant droplet underneath an inclined substrate, and Fig. 3(*b*) highlights the relevant forces at the contact line. The base of the drop is assumed to be circular, as shown in Fig. 3(*c*), and its volume is calculated using the spherical cap approximation, as shown in Fig. 2(*b*).[4] With known advancing and receding contact angles, the geometric reconstruction

[3]Typically droplet mergers happen in a time scale of 5–300 ms, depending on their respective sizes and thermophysical properties [30–32]. In contrast, the entire experiment of dropwise condensation, from a virgin surface to the first fall-off or a slide-off is typically of the order of one hour. This justifies our assumption of 'instantaneous coalescence.

[4]There is some conflict in the calculation of volume and its experimental validation for sessile drops on inclined surfaces, as reported in [40–43]. Some reports [40–42] suggest that approximating the drop shape as a spherical cap can lead to 10%–25% error in volume. Based on experimental evidence, others [43] believe that such an approximation is quite valid. To the best of the knowledge of the authors, there is no corresponding literature on the calculation of pendant drop volumes. Therefore, the spherical cap approximation has been used in the present work.

Downloaded 08 Nov 2010 to 202.3.77.11. Redistribution subject to ASME license or copyright; see http://www.asme.org/terms/Terms_Use.cfm

of the entire droplet is possible.

The retention forces perpendicular and parallel to the substrate are calculated as

$$F_{r\|} = 2\int_0^{\pi} \sigma \cos\theta \cos\phi \cdot r_b \cdot d\phi \tag{14}$$

$$F_{r\|} = \sigma r_b\left[\frac{\pi}{2\pi - \theta_{rcd} - \theta_{adv}}\{\sin(2\pi - \theta_{rcd}) - \sin\theta_{adv}\} + \frac{\pi}{\theta_{adv} + \theta_{rcd}}\{\sin\theta_{rcd} + \sin\theta_{adv}\}\right] \tag{15}$$

As noted earlier, the drop is assumed as a segment of a sphere with a contact angle θ_{avg}, where θ_{avg} is evaluated at the base of the drop. Hence,

$$\theta_{avg} = (\theta_{rcd} + \theta_{adv})/2 \tag{16}$$

The volume of the equivalent spherically capped droplet is given by

$$V_{sc} = \frac{\pi \cdot r_b^3(2 - 3\cos\theta_{avg} + \cos^3\theta_{avg})}{3\sin^3\theta_{avg}} \tag{17}$$

The force component due to gravity that is parallel to the substrate is

$$F_{g\|} = \frac{\pi r_b^3(2 - 3\cos\theta_{avg} + \cos^3\theta_{avg})}{3\sin^3\theta_{avg}}\rho \cdot g \sin\alpha \tag{18}$$

Finally, the critical radius of the droplet at slide-off on the inclined substrate is calculated as

$$r_{crit} = \sqrt{\left(\frac{3\sin^3\theta_{avg}}{\pi(2 - 3\cos\theta_{avg} + \cos^3\theta_{avg})}\right)\left[\frac{\pi}{2\pi - \theta_{rcd} - \theta_{adv}}\{\sin(2\pi - \theta_{rcd}) - \sin\theta_{adv}\} + \frac{\pi}{\theta_{adv} + \theta_{rcd}}\{\sin\theta_{rcd} + \sin\theta_{adv}\}\right]\left(\frac{\sigma}{(g\sin\alpha)(\rho_l - \rho_v)}\right)} \tag{19}$$

The surface tension component perpendicular to the inclined substrate is calculated as

$$F_{r\perp} = 2\int_0^{\pi} \sigma \sin\theta \cdot r_b \cdot d\phi \tag{20}$$

$$F_{r\perp} = 2\sigma \cdot r_b\left(\frac{\pi}{\pi - \theta_{rcd} - \theta_{adv}}\right) \cdot (\cos\theta_{rcd} + \cos\theta_{adv}) \tag{21}$$

The gravity force component perpendicular to the substrate is

$$F_{g\perp} = \frac{\pi r_b^3(2 - 3\cos\theta_{av} + \cos^3\theta_{av})}{3\sin^3\theta_{av}}\rho \cdot g\cos\alpha \tag{22}$$

The maximum radius of the drop at fall-off is obtained by balancing the forces perpendicular to the substrate as

$$r_{max} = \sqrt{\left(\frac{6(\sin^3\theta_{avg})(\cos\theta_{rcd} + \cos\theta_{adv})}{(2 - 3\cos\theta_{avg} + \cos^3\theta_{avg})(\pi - \theta_{rcd} - \theta_{adv})}\right)\left(\frac{\sigma}{(g\cos\alpha)(\rho_l - \rho_v)}\right)} \tag{23}$$

On an inclined surface, critical sized droplets first begin to slide-off, rather than fall, as on a horizontal substrate. Criticality is achieved by direct condensation growth or, alternatively, by coalescence with the adjoining drops. Thus, depending on the length scale of the substrate and the time scales of direct growth and growth due to coalescence, there are various possibilities on an inclined substrate. These include the following:

(i) Slide-off criticality is achieved, and during the entire slide-off on the substrate, fall-off criticality is not achieved.
(ii) Slide-off criticality is achieved, and during the slide-off on the substrate, fall-off criticality is also achieved before the droplet traverses the complete substrate length scale.

Both these possibilities have been incorporated in the mathematical model.

During slide-off, the body forces accelerate the droplets, and in the process many droplets on the path are swept away. The acceleration of the droplet is calculated by computing force components. Those parallel to the substrate are

(i) gravity force, $F_{g\|}$
(ii) force due to shear at the wall, F_s
(iii) retention force due to surface tension, $F_{r\|}$

A linear velocity distribution is assumed inside the moving drop, and the maximum velocity is taken to appear at its center of mass [33,34,44,45], which is at a distance of L from the substrate. The velocity gradient and shear stress are thus calculated as

$$\frac{du}{dy} = \frac{U}{L} \tag{24}$$

$$\tau = \mu_l\frac{du}{dy} = \mu_l\frac{U}{L} \tag{25}$$

The viscous force on the droplet is calculated as

$$F_s = \tau \cdot \pi \cdot r_b^2 \tag{26}$$

From these forces, the acceleration and velocity of the droplet are calculated as

$$a = \frac{F_{g\|} - F_s - F_{r\|}}{m} \tag{27}$$

Downloaded 08 Nov 2010 to 202.3.77.11. Redistribution subject to ASME license or copyright; see http://www.asme.org/terms/Terms_Use.cfm

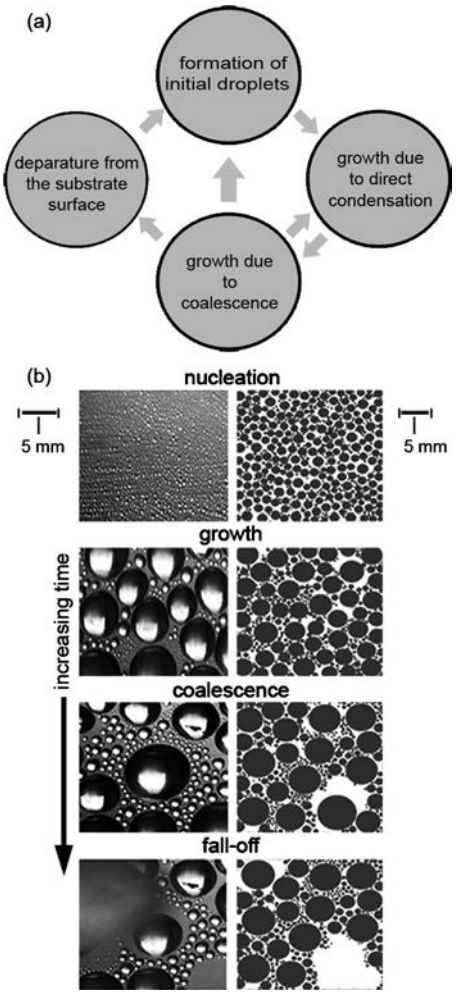

Fig. 4 (*a*) The cycle of major physical processes observed in the pendant mode of dropwise condensation on a horizontal substrate. (*b*) Qualitative comparison of experimental images of dropwise condensation on silanated glass substrate of area 25×25 mm² (coated with octyl-decyl-tri-chloro-silane, $C_{18}H_{37}C_{13}Si$) with corresponding images generated by simulation. The hazy patch seen in the top-left section of the last experimental image is due to the fact that the droplet has fallen on the viewing glass (view A) through which images are being recorded.

$$U_{\text{curr}} = U_{\text{prev}} + a \cdot dt \tag{28}$$

Finally, closure is obtained by externally supplying the wettability characteristics of the substrate, i.e., its average contact angle for a horizontal substrate and the advancing-receding angles for the inclined substrate, both from experimental data. Using these equations, the entire dropwise condensation process is simulated underneath an inclined substrate from initial nucleation to a dynamic quasi-steady state.

3.3 Model Assumptions. The following are the main assumptions considered during the development of the mathematical model.

1. Nucleation sites are randomly distributed on the surface. The initial nucleation site density of 10^9 m^{-2} is assumed [12].
2. The thermodynamically constrained smallest radius is taken as the minimum radius in the simulation. Initially, the substrate is virgin, and all nucleation sites are instantaneously occupied by the droplet of minimum radius.
3. Prior to reaching the critical volume for fall-off or slide-off, all drops are located at the weighted center of mass of the coalescing droplets.
4. Heat transfer resistance arises due to the liquid-vapor interface, curvature, and conduction, driven by subcooling of the substrate. Constriction resistance and convective transport of heat inside the drop are neglected.
5. The accommodation coefficient is taken to be 0.02 for water and 0.21 for sodium [3]. Although literature suggests that the accommodation coefficient is also a function of temperature, we have not changed its value in the simulations.
6. Droplet coalescence is assumed to be instantaneous and smooth (refer to footnote 4); inertia effects and change in the shape of the droplet due to acceleration are neglected.
7. An equivalent spherical cap approximation has been incorporated to model droplet shapes.
8. The dynamic variation in contact angle is neglected. For a particular surface-liquid combination, its value is taken to be constant and prescribed.
9. Partial fall-off of droplets is neglected; complete volume of the critical drop is removed.
10. The entire substrate is assumed to be at constant temperature; any local variation due to drop dynamics is neglected.

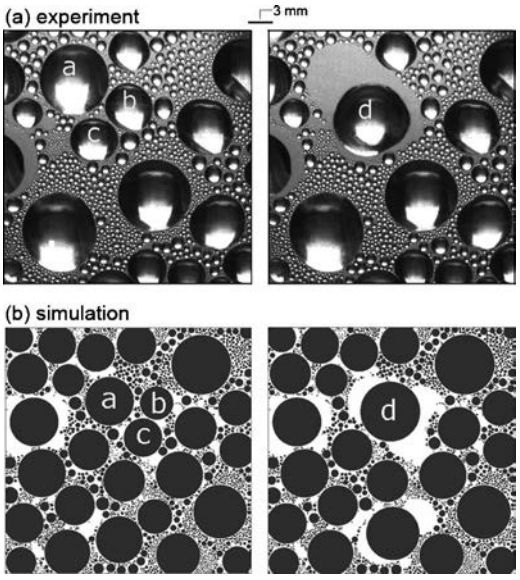

Fig. 5 Sequence of two images observed during experiment and corresponding simulation, showing coalescence of three droplets a, b, and c, resulting in the formation of a composite drop d

4 Results and Discussion

Dropwise condensation of distilled and de-ionized water, underneath a horizontal substrate and an inclined substrate having an angle of inclination of 15 deg, has been carried out on a glass substrate, which is coated by octyl-decyl-tri-chloro-silane ($C_{18}H_{37}C_{13}Si$). The saturation temperature is maintained at 27°C in all experiments with a cold substrate always maintained at 22°C. The static contact angle of water underneath the chemically textured substrate was measured to be 96 ± 0.5 deg for the droplet volume range of 50–100 μl. The experimental process is simulated by the mathematical model for both horizontal and inclined arrangements of the substrate, subject to features, assumptions, and limitations outlined in Sec. 3.3. Section 4.1 first reports the experimental observations of dropwise condensation on chemically textured horizontal and inclined surfaces. The data are compared against the simulation model presented in Sec. 3. After validation, simulations are performed for the range of parameters not covered in the experiments. Here, the effect of the static contact

Downloaded 08 Nov 2010 to 202.3.77.11. Redistribution subject to ASME license or copyright; see http://www.asme.org/terms/Terms_Use.cfm

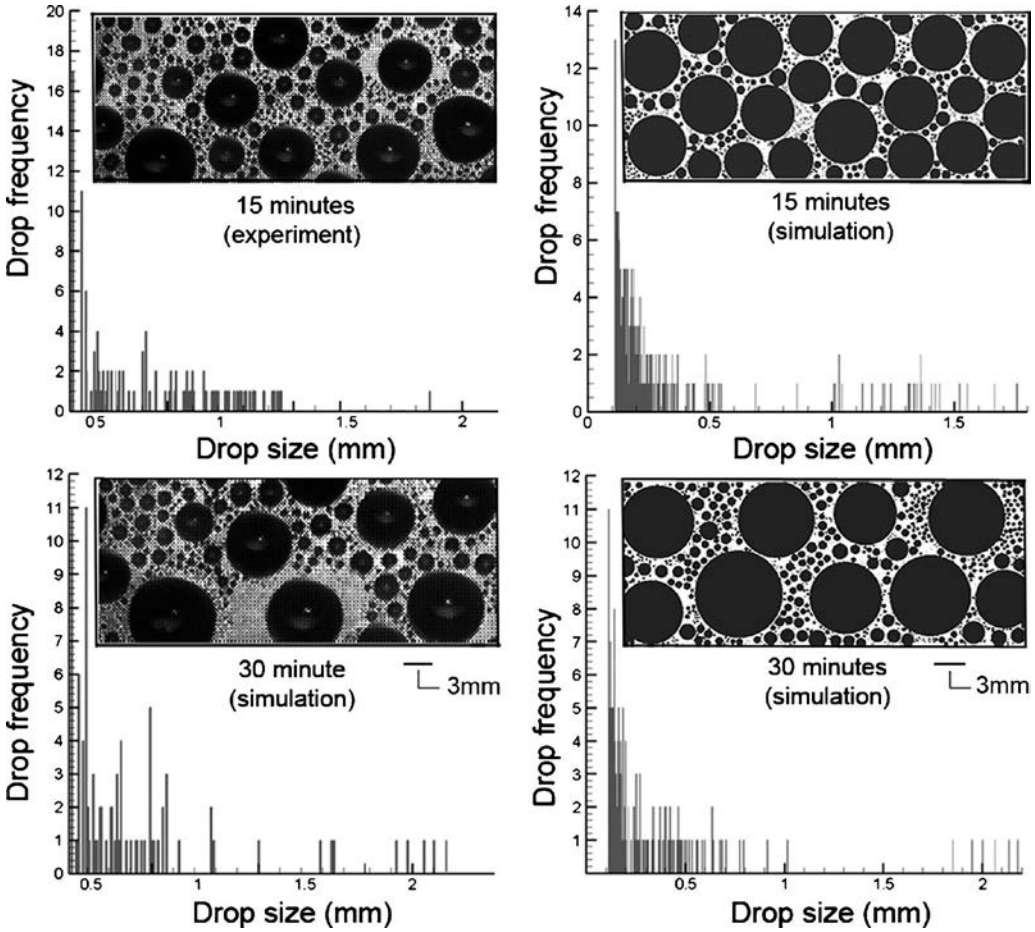

Fig. 6 Visual and statistical comparison of experimental and simulated spatial drop distribution patterns and the corresponding histograms of droplet frequency at the dynamic steady state

angle, thermophysical properties of the working fluid, physicochemical properties of the substrate, and the angle of inclination of the substrate are considered.

4.1 Experimental Observations and Comparison With Simulation. The experimental results and the corresponding numerical simulation of condensation of water at saturation temperature of 27°C ($\Delta T_{sat}=5°C$) are compared both on qualitative and quantitative terms. Major results are summarized in Figs. 4–11. Figure 4(*a*) schematically depicts the major observable processes of dropwise condensation underneath a horizontal substrate. These are nucleation, growth, coalescence, and fall-off of droplets. Figure 4(*b*) visually and qualitatively highlights these processes, as observed experimentally (view A in Fig. 1(*b*)) and captured in the computer simulation. The statistical nature of the overall process, with multiple generations of droplets in different stages of their respective growth phase and present simultaneously on the substrate, is clearly visible. Contrary to the perfect circular footprints of the droplet bases assumed in the simulation, local phenomena such as pinning of the contact line [10], capillary waves, contact line inertia during droplet merging, and the dynamics of the liquid-vapor interface cause deviations that are observable in the experiments. Specifically, droplet pinning and the noncircular base of the footprint can be clearly seen in the experimental images. Thus, the mathematical model can be further refined to cover local disturbances. However, major phenomena related to dropwise condensation underneath horizontal substrates are well simulated by the model.

Figure 5 depicts coalescence of three drops (marked as a, b, and c) as observed during the experiment and as revealed in the simulation. In the simulation, the center of the new resulting drop (after coalescence, i.e., drop d) is determined by a mass weighted average of centroids of constituent droplets before coalescence (i.e., droplets a, b, and c). The assumption that the coalesced volume takes up the weighted center of mass of the original droplets is vindicated by this representative comparison. The merger results in the exposure of virgin areas around the drop where renucleation of the new generation droplets will commence. Droplet mergers bring about near instantaneous changes in the total area coverage as well as the drop size distribution. A closer look at the edges of the droplets during experiments, especially the larger droplets, also reveals that the shapes of their bases are not exactly circular, showing local pinning phenomenon of the contact line at certain locations (e.g., see drop d in the experimental image). As droplets merge, experimental images show that it takes a certain finite time (of the order of 0.1–300 ms, depending on the respective sizes of the coalescing droplets) for the surface and body forces to redistribute the fluid in the coalesced drop and come to the state of minimum possible energy level; the new contact line shrinks and tends to be as circular as possible in a finite relaxation time; local pinning can distort its circularity.

Figure 6 shows the spatial drop size distributions underneath the horizontal substrate at 15 min and 30 min, respectively, after the commencement of the condensation process. No fall-off has yet taken place. The strong temporal variation in size distribution of droplets is clearly visible. As can be seen, after a 15 min time interval, the distribution shows moderately sized droplets with the maximum diameter of about ~2.0 mm. As time progresses, droplets merge, exposing virgin areas; an increase in the number den-

Downloaded 08 Nov 2010 to 202.3.77.11. Redistribution subject to ASME license or copyright; see http://www.asme.org/terms/Terms_Use.cfm

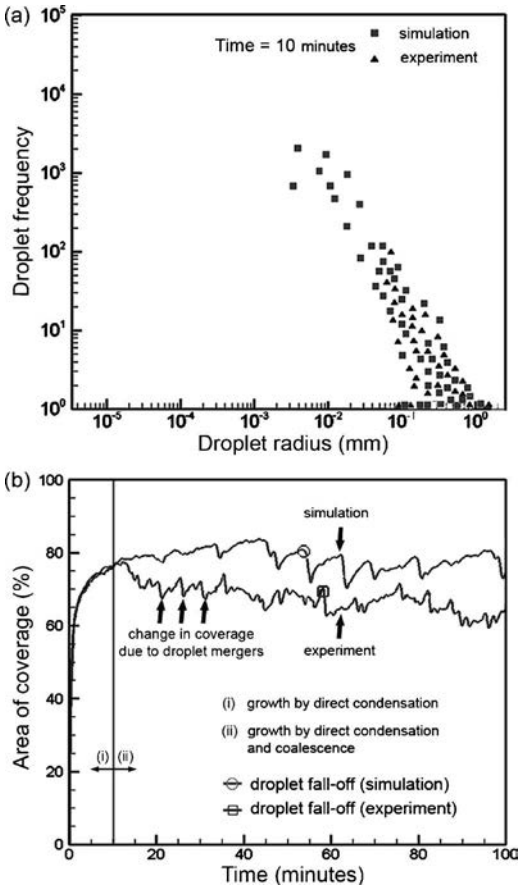

Fig. 7 (*a*) Drop size distribution from experiments and simulation at a time of 10 min after the commencement of dropwise condensation. (*b*) Time-wise variation in the area coverage of droplets over the substrate.

sity of very small droplets (below ~0.5 mm) is clearly visible at 30 min. In addition, the number density of larger droplets (greater than ~2.0 mm has increased substantially). The simulated histograms are denser than the experimental counterpart due to the loss

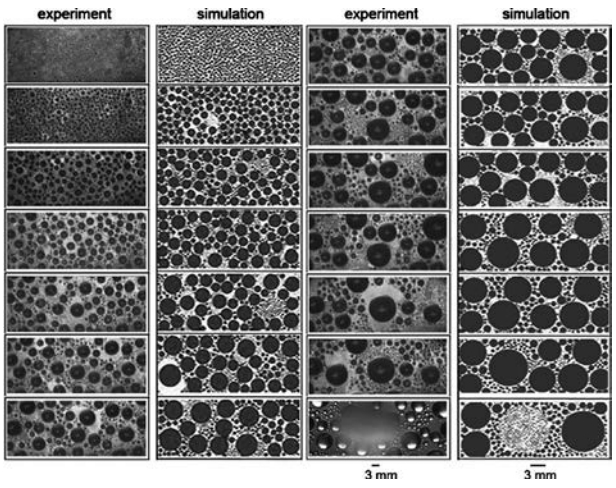

Fig. 8 Comparison of experiments and corresponding simulation for the complete sequence of dropwise condensation process, from the appearance of drops of minimum radius to the drops of critical radius underneath a horizontal silanated glass substrate of 25×10 mm^2 area

of information in experimental data during image processing of droplets below about 0.1 mm. For the same reason, the experimental and simulation histograms of the 15 min data are more dissimilar than those at 30 min. Initially, as condensation commences, the number of smaller sized droplets is quite large. At later times, droplets of higher diameter are greater in number, as noted earlier, and are captured well by the digital camera. In the latter part of the process, the growth is chiefly dominated by coalescence, and the number density distribution shifts toward larger sized drops.

Figure 7(*a*) compares the experimental and simulated droplet frequencies plotted as a function of the drop radius 10 min after the commencement of the condensation process. The experimental fall-off time for the first drop was approximately 58–62 min, while the simulation predicted a number in the range of 48–54 min. It is clear that drops whose radius is less than ~0.1 mm have not been recorded by the camera. The corresponding range of drop sizes that could be included in the simulation is 10^{-3}–1.0 mm. Although the order of magnitude of $r_{\min}$ (at time $t=0$) is $\sim10^{-4}$ mm, nearly all the original drops have since grown to the order of 10^{-3} mm at 10 min, mostly by direct condensation growth. Droplet coalescence has not yet started, as can be clearly seen in Fig. 7(*b*), where the temporal change in area coverage of drops is presented. Initially, there is a rapid increase in the coverage, and later, it approaches a dynamic quasi-steady state. Two distinct zones clearly seen in the experimental and simulation data are (i) growth due to direct condensation in the initial period and (ii) growth due to coalescence. Large local fluctuations in area coverage represent time instants when drops either coalesce to form larger drops or a large drop fall-off/slide-off. The fact that smaller drops could not be accounted due to imaging limitations explains the higher values of coverage area in simulation (73.1%) compared with experimental data (64.5%).

Figure 8 shows the complete sequence of experimental and simulated drop distributions, from the appearance of drops of minimum radius to the formation of drops of critical radius, underneath a horizontal substrate of 25×10 mm^2 area. The first image is at a time instant of 1 min, and thereafter the images are at 4 min intervals. The last image is presented at 59 min for the experiment and 50 min for the simulation. For this experiment, the first fall-off occurred at 58.5 min, while in the corresponding simulation, the first instance of fall-off was observed at 48 min and 10 s. This discrepancy may arise due to the following factors: (a) Noncondensable gases in the experimental chamber can deteriorate the heat transfer coefficient and delay the drop growth rate. (b) The local effects of pinning and contact line dynamics lead to higher frictional stresses, which enhance surface forces and delay fall-off. The comparisons shown in Fig. 8 for a horizontal substrate, however, show that the simulator satisfactorily captures the major processes of dropwise condensation, both from qualitative and quantitative standpoints.

4.1.1 Inclined Substrate. Various attributes of dropwise condensation of water at a saturation temperature of 27°C ($\Delta T_{\text{sat}}=5$°C) underneath an inclined substrate (15 deg from horizontal; $\theta_{\text{adv}}=111$ deg, $\theta_{\text{rcd}}=81$ deg), recorded in experiments and observed in numerical simulation, are shown in Figs. 9–11.

Major physical processes observed on an inclined substrate are similar to those of the horizontal substrate, except that the simple fall-off mechanism is replaced by a more complex combination of slide-off and fall-off. On an inclined substrate, a critically sized sliding droplet, while sweeping other droplets on its path, may either (i) reach the end of the substrate without falling off or (ii) acquire enough mass to be pulled in the downward direction, thus falling off from the substrate before actually reaching the edge of the substrate. The scenario realized will depend on the rate of growth of the drop, coalescence, and the length of the substrate itself. The other physical processes of nucleation, direct condensation growth, coalescence, and merger dynamics are quite similar

Downloaded 08 Nov 2010 to 202.3.77.11. Redistribution subject to ASME license or copyright; see http://www.asme.org/terms/Terms_Use.cfm

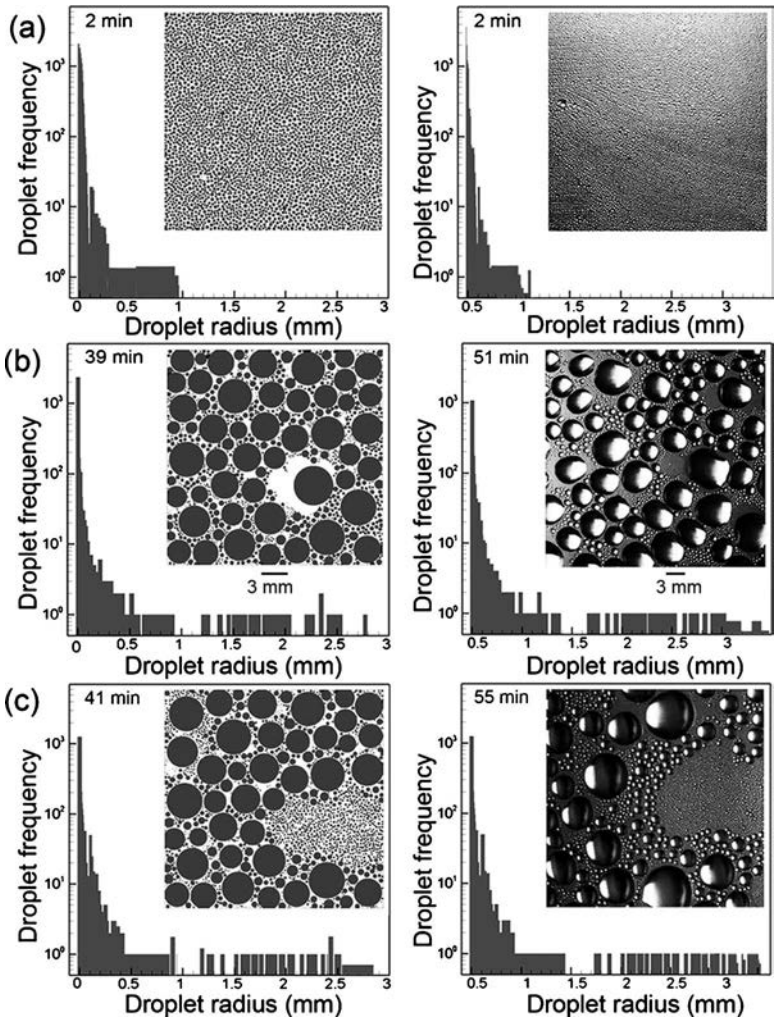

Fig. 9 Size distribution of drops condensing underneath an inclined (15 deg) silanated glass substrate of size 25×25 mm^2 as recorded in experiments and in the simulation: (*a*) at time=2 min from the commencement of dropwise condensation, (*b*) at critical state of slide-off, and (*c*) just after a complete sweeping action is completed by a sliding drop

to those of the horizontal substrate. The fact that the gravity vector now acts at an angle to the growing droplets leads to unsymmetrical drop deformation. The contact angle hysteresis plays a role in the static force balance, as explained in Sec. 3.

Figure 9 depicts the experimental images and histograms of droplet frequency along with the corresponding simulation data for the hydrophobic surface of 15 deg inclination. The critical stage of slide-off is also pictorially compared; a discrepancy in the actual time of slide-off in experiments as opposed to simulation is again observed. Soon after slide-off, virgin areas are created, nucleation sites are exposed, and renucleation commences, as shown in Fig. 9(*c*). Moreover, repeated removal of drops leads to the time averaged area of coverage being smaller for the inclined substrate when compared with the horizontal. At the instant of the first slide-off, the area coverage is 58.8% in simulation and 49.5% from experiments. The discrepancy is again primarily attributed to the loss of data pertaining to small sized droplets during experimental observations.

Figures 10 and 11 show the complete temporal sequence of events on the inclined substrate. Unlike a horizontal substrate, the drop dynamics on an inclined substrate is unique because the criticality of droplet motion and the series of events soon thereafter (sweeping and/or fall-off) happen extremely quickly leading to a sudden reduction in area coverage. It is clear from the histograms of Fig. 9 that the drop slide-off underneath the inclined substrate occurs earlier than the corresponding time instant of fall-off underneath a horizontal substrate. Figure 11 depicts the complex sequence of slide-off, rapidly followed by sweeping, fall-off, and renucleation. After the first instance of slide-off, it is interesting to note that the subsequent slide-offs and sweeping actions occur at a greater frequency. The mathematical model satisfactorily captures these processes.

4.2 Parametric Study. The effect of the static contact angle, namely, the wettability and substrate inclination, and the effect of the thermophysical properties of the working fluid on dropwise condensation patterns are parametrically explored in the present section at a condensation temperature of 30°C and a cold substrate temperature of 25°C. The mathematical model of Sec. 3 is used for data generation. During simulation, the nucleation site density has again been taken as 10^9 m^{-2}.

The effect of the wettability of the condensing liquid on the substrate is explored in Fig. 12(*a*), where the spatial drop distribution underneath a horizontal chemically textured substrate of 20×20 mm^2 area, just before fall-off, is pictorially depicted. A reduction in wettability increases the contact angle and leads to a smaller base circle of the drop and, therefore, smaller surface forces holding the drop. Thus, two effects are clearly visible. (i)

Downloaded 08 Nov 2010 to 202.3.77.11. Redistribution subject to ASME license or copyright; see http://www.asme.org/terms/Terms_Use.cfm

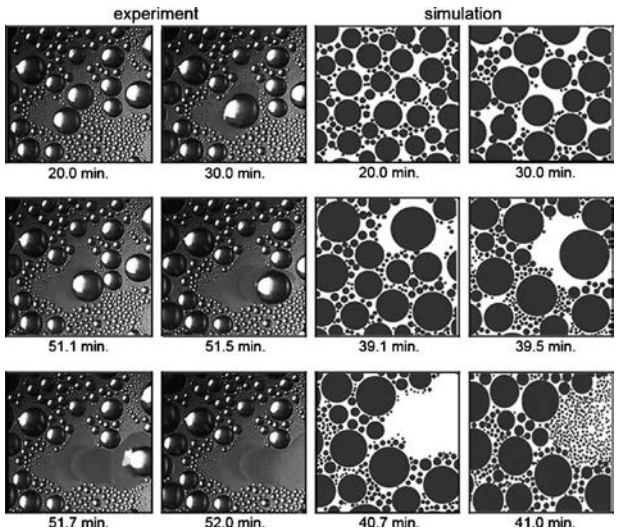

Fig. 10 Various temporal stages of droplet condensation on the inclined substrate (15 deg) recorded during experiments and simulation. The commencement of sliding and sweeping actions of the drop as it gathers mass during transit and renucleation of the virgin exposed surface, when the sweeping action is complete, are clearly seen.

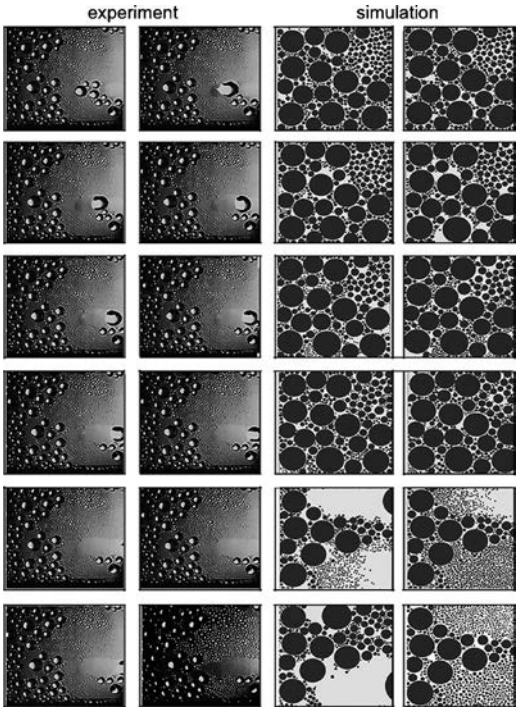

Fig. 11 Sequence of images from experiments as well as simulation showing drop slide-off and the subsequent sweeping action on a 15 deg inclined 25×25 mm^2 substrate. A dynamic steady state in the process has been achieved. Once slide-off commences, the drop quickly gathers mass during the sweeping action and subsequently falls off.

The droplet volume at the time of fall-off is smaller. The area coverage of the drops, seen in Fig. 12(*b*), is smaller as well. The quasi-steady state area coverage varies with contact angle from 73.3% for 90 deg, 67.1% for 105 deg, and 52.4% for 120 deg. (ii) With increasing contact angle, the drops achieve fall-off criticality earlier in the cycle, as shown in Fig. 12(*c*). All other conditions remaining unchanged, the fall-off time for a pendant drop is seen

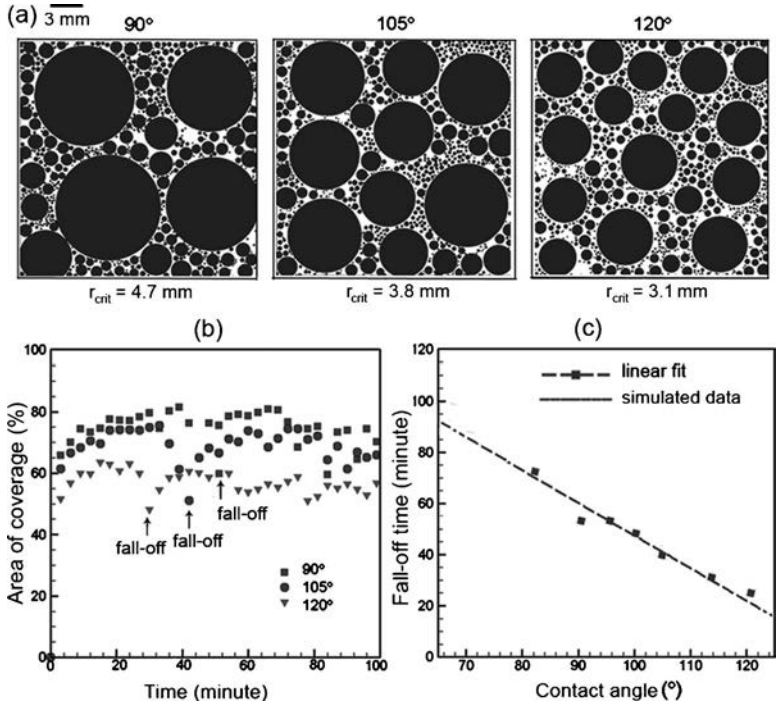

Fig. 12 Effect of wettability: (*a*) Simulated spatial droplet distribution just before fall-off of a drop underneath a horizontal substrate of 20×20 mm^2 area for contact angles of 90 deg, 105 deg, and 120 deg. (*b*) Temporal variation in coverage area of drops. (*c*) Fall-off time of the drop as a function of the contact angle (for all cases working fluid: water; T_{sat}=30°C, ΔT_{sat}=5°C).

Downloaded 08 Nov 2010 to 202.3.77.11. Redistribution subject to ASME license or copyright; see http://www.asme.org/terms/Terms_Use.cfm

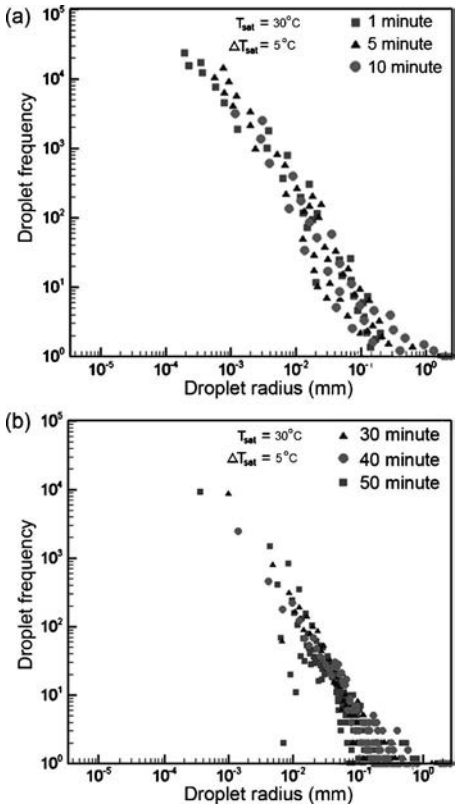

Fig. 13 ((*a*) and (*b*)) Temporal variation in drop size distribution for condensing water vapor underneath a horizontal silanated glass substrate (contact angle of 90 deg). For clarity, data for 1–10 min are separately plotted from the data of 30–50 min. The fall-off time for the first drop was equal to 48 min in this simulation. Immediately after fall-off (at 50 min), very small drops reappear because of the virgin area created after fall-off.

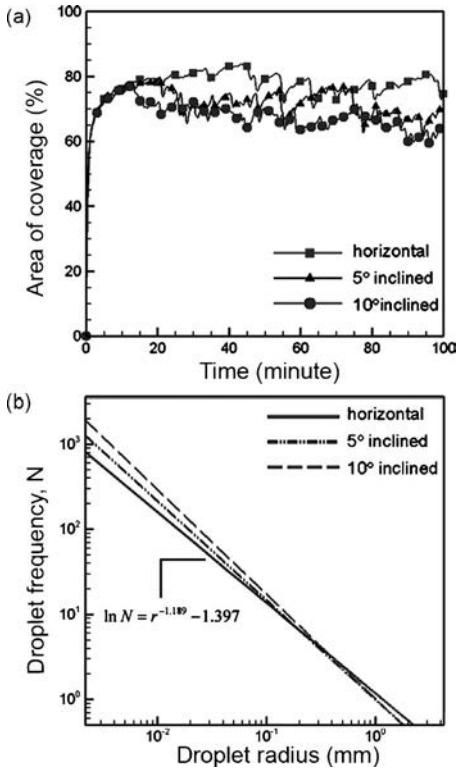

Fig. 14 Effect of substrate inclination: (*a*) Temporal variation in area coverage of drops during condensation of water in the pendant mode. (*b*) Drop size distribution just before fall-off (for horizontal substrate) or slide-off (inclined substrate). For this simulation, the wettability of the substrate is such that θ_{adv} =106 deg and θ_{rcd}=74 deg for angle of inclination of 5 deg and θ_{adv}=110 deg and θ_{rcd}=61 deg for angle of inclination of 10 deg; the droplet is assumed to be hemispherical on a horizontal surface; T_{sat}=30°C, ΔT_{sat}=5°C.

to be a linear function of the contact angle.

Figure 13(*a*) shows the frequency (namely, the number of drops) as a function of the drop radius, 10 min after commencement of condensation. At later times, drops of higher sizes are to be seen. For the present simulation, the fall-off time of the first drop was 48 min. Figure 13(*b*) shows that very small droplets nucleate on the substrate at $t=50$ min, immediately after the first drop falls off at $t=48$ min.

The effect of substrate inclination on the temporal distribution of area coverage is presented in Fig. 14(*a*). Inclination of the substrate facilitates easier movement of drops by sliding, leading to a droplet sweeping action. Therefore, the effective steady state coverage is smaller for inclined substrates, changing from 67.4% for the substrate with 10 deg inclination to 71.2% for 5 deg inclination, and 76.1% for a horizontal substrate. At the instant of the first fall-off (for the horizontal substrate) and the first slide-off (for the inclined substrate), Fig. 14(*b*) depicts the drop size distribution as a function of radius for various inclination angles. The distribution follows a power law with the negative slope increasing with the substrate angle, reflecting the repeated appearance of small drops at fresh nucleation.

For a given degree of subcooling ($\Delta T_{sat}=5°C$), the effect of saturation temperature on drop departure time is shown in Fig. 15 (working fluid: water). It is seen that increasing the saturation temperature reduces the fall-off time (and hence the size of the largest drop), indicating an increase in the overall heat transfer coefficient. The diffusional thermal resistance within the drop is a major limiting factor of condensation heat transfer. Hence, increasing the saturation temperature increases the thermal conductance of the water drop in the applicable range of the simulation. A marginal increase in the overall resistance is also noticed due to a reduction in the interfacial heat transfer coefficient; it essentially proves to be inconsequential as the overall thermal resistance is dominated by the conduction resistance of the droplet [14,46,47].

The effect of Prandtl number on convective heat transfer is well

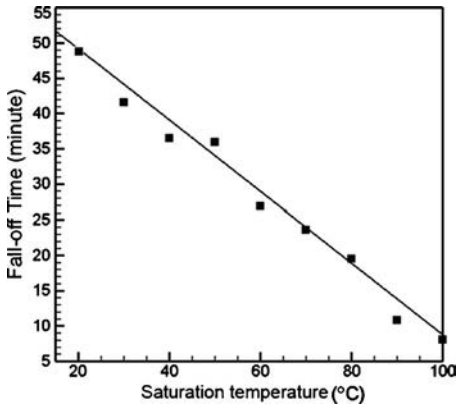

Fig. 15 Variation in drop departure time (time required for first fall-off) on a horizontal substrate with respect to the saturation temperature. Fluid employed is water, subcooling ΔT_{sat}=5°C, contact angle=90 deg, and nucleation site density=10^9 m^{-2}. For a given nucleation site density, the fall time has an uncertainty of ±3 min, depending on the random assignment of initial droplet centers on the substrate.

Downloaded 08 Nov 2010 to 202.3.77.11. Redistribution subject to ASME license or copyright; see http://www.asme.org/terms/Terms_Use.cfm

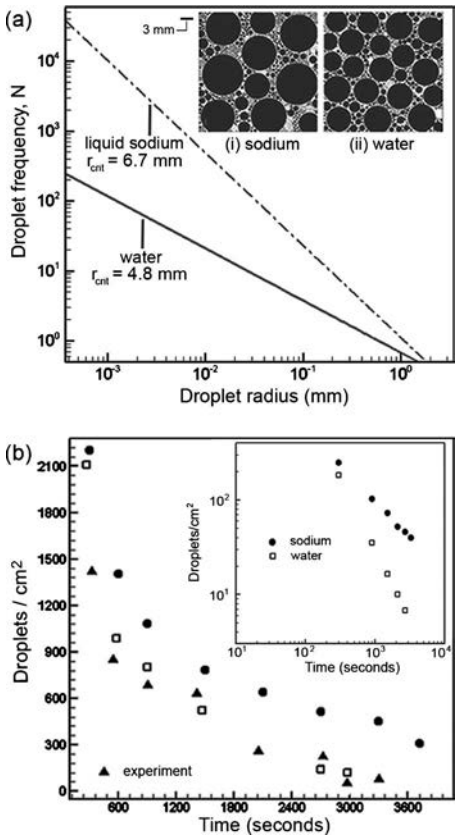

Fig. 16 (*a*) Spatial drop distribution for condensation underneath horizontal stainless steel substrate just before fall-off for (i) liquid sodium (T_{sat}=342°C, ΔT_{sat}=5°C, θ=108 deg) and (ii) water (T_{sat}=30°C, ΔT_{sat}=5°C, θ=73 deg), with the corresponding pictorial depiction in the inset. For liquid sodium, the fall-off time is 66 min, and for water it is 48. (*b*) The temporal variation in the number density of drops of water and sodium from the commencement of condensation until 60 min.

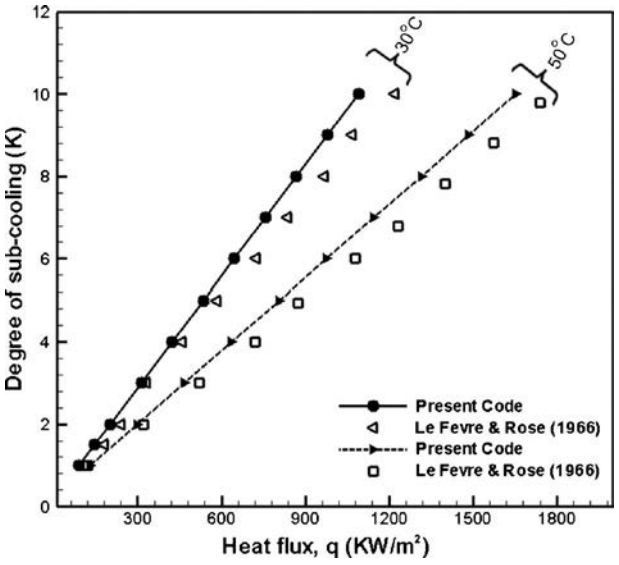

Fig. 17 Variation in heat transfer coefficient for dropwise condensation of water on a horizontal substrate at T_{sat}=30°C and T_{sat}=50°C with the degree of subcooling. The results from the present simulator are compared with the prediction model of Le Fevre and Rose for dropwise condensation of water on a promoter layer, as reported by Rose [1].

documented. In many situations, a singular behavior is observed for low Prandtl number systems, for example, liquid metals where $Pr \sim 10^{-2}$. Moreover, condensation of liquid metals also plays an important role in many engineering processes.

The results obtained by extending the present model to dropwise condensation of liquid metals are depicted in Figs. 16(*a*) and 16(*b*). The spatial distributions of drops underneath a horizontal substrate, just before fall-off, are compared in Fig. 16(*a*) for water and liquid sodium. Owing to the higher surface tension of liquid sodium, the departing drop size, as governed by critical Bond number, is considerably larger for sodium, being ~6.7 mm, as against ~4.8 mm for water. In liquid metals, a large number of small drops are present on the substrate, whereas the number density of small drops for condensing water is smaller (see inset of Fig. 16(*a*)). Figure 16(*b*) shows the temporal variation in the number density of drops of water and sodium from the commencement of condensation until 60 min. As condensation proceeds from time t=0, the droplet distribution and density continuously change; this variation follows a power law with time ($t \sim^{-\alpha}$) with α=1.54 for water and 0.76 for sodium. Experimental data for water condensing on chemically textured silanated glass are also shown for comparison. The inset shows these data on a log-log scale.

The variation in the average heat transfer coefficient for dropwise condensation of water with respect to the degree of subcooling (T_{sat}-T_w) at condensation temperatures 30°C and 50°C, respectively, on a horizontal chemically textured substrate is shown in Fig. 17. To calculate the average heat transfer coefficient, the simulation is continued for a period of 3 h. The amount of condensate collected, namely, the net summation of the fall-off volume in the entire period is tracked to determine the total latent heat transfer. The comparison of the present simulation with the theory put forward by Le Fevre and Rose for dropwise condensation of water on a monolayer promoter layer, as reported by Rose [1], is also shown.

The variation in the critical angle of inclination for the commencement of sliding with respect to the droplet radius for various liquid metals is shown in Fig. 18(*a*). The advancing and receding angles are taken to be known quantities for the purpose of simulation. For a given drop radius, the ordinate represents the angle that the substrate makes with the horizontal. At this stage of criticality, the weight of the drop exceeds the surface force holding it, resulting in either a fall-off or a slide-off. Increasing the angle of substrate inclination decreases the radius at which droplet slide-off commences. The critical angle of inclination also depends on the surface tension of the liquid; larger surface tension liquids have a greater critical inclination angle before sliding starts. The effect of the contact angle hysteresis on the critical angle of inclination is seen in Fig. 18(*b*). As the contact angle hysteresis is reduced, the critical angle of inclination for sliding motion reduces.

5 Conclusions

The heat transfer coefficient during dropwise condensation is two to three orders of magnitude higher than in filmwise condensation and is a preferred mode in many processes. Prediction of the heat transfer coefficient in dropwise condensation poses many challenges. Most heat transfer models proposed in the literature require a priori knowledge of the drop size distribution and the number density of condensing droplets after cyclic quasi-steady state is reached. These data are also required to calculate the average shear stress on the substrate arising from continuous cycles of dropwise condensation. Comprehensive inclusion of all forces affecting the droplet dynamics is thus essential for the prediction of transport properties of interest.

Against this background, a detailed simulation of dropwise condensation is proposed from first principles. The simulator is applicable for condensation underneath horizontal and inclined substrates. It accounts for growth by direct condensation and

Downloaded 08 Nov 2010 to 202.3.77.11. Redistribution subject to ASME license or copyright; see http://www.asme.org/terms/Terms_Use.cfm

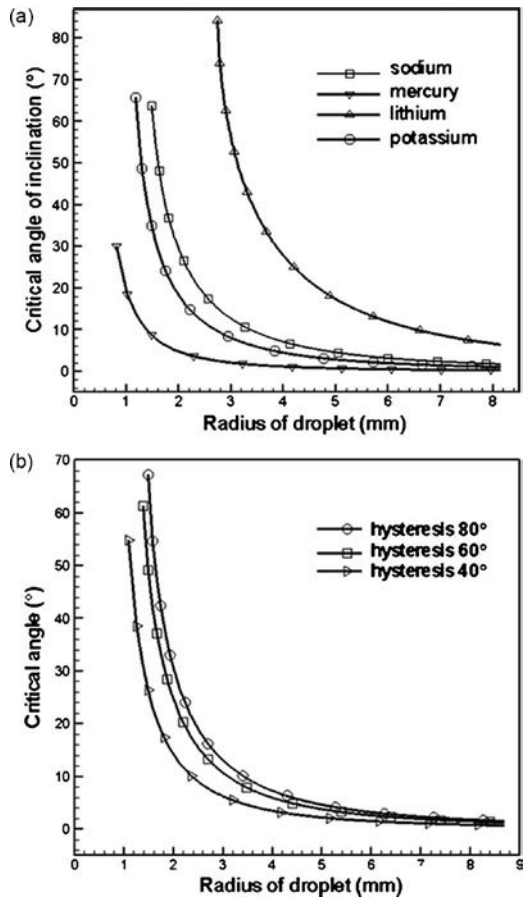

Fig. 18 (*a*) Critical angle of inclination of the substrate as a function of the drop size with respect to fall-off (horizontal substrate)/slide-off (inclined substrate). (*b*) Effect of contact angle hysteresis on the critical radius of the drop.

coalescence, subsequently resulting in drop motion due to force imbalances. Specific experiments have been carried out on a salinated glass substrate to understand the mechanisms of droplet growth, coalescence, and fall-off and slide-off behaviors. The data recorded in experiments are compared with those of the simulation. Post-validation, the simulator is extended for contexts not covered by the experiments. The effects of the contact angle, contact angle hysteresis, inclination of the substrate, thermophysical properties of the working fluid, and the saturation temperature of condensation are investigated. The following conclusions have been arrived at in the present study:

1. The mathematical model presented captures the major constituents of the dropwise condensation process quite satisfactorily. While there may be many reasons for the discrepancy between the predictions of the model and experimental data, some of which have been discussed in the paper, looking at the experiments closely we do believe that highly localized three-phase contact line dynamics, related to the anisotropic distribution of surface energy and surface roughness distribution, are likely candidates for further scrutiny and need to be incorporated in the model.
2. Essentially two distinct growth phases of droplet growth are observed: (a) growth due to direct condensation and (ii) growth primarily due to coalescence. The area fraction covered by the drops increases as the drops grow and finally achieves a dynamic quasi-steady state after many cycles of coalescence and fall-off/slide-off.
3. An increase in static contact angle (decrease in wettability of the substrate) reduces the droplet area coverage. Reduction of coverage is also observed by increasing the substrate inclination.
4. A decrease in wettability also results in earlier fall-off (horizontal substrate)/earlier slide-off (inclined substrate). In all cases, the simulations predict earlier fall-off than in experiments.
5. Inclining the substrate results in a larger number of small drops and hence in a higher heat transfer coefficient. This is because the resistance to heat transfer per unit area is smaller in smaller drops compared with larger drops.
6. At a higher saturation temperature, the rate of growth of the drop is higher. Heat transfer coefficient increases with an increase in the degree of subcooling of the substrate and is a strong function of the Prandtl number of the fluid. This is primarily due to the fact that diffusional resistance of the liquid drop constitutes the major thermal resistance in the flow of heat from the vapor to the substrate.
7. The critical radius of droplet, at which commencement of sliding takes place, is a function of the thermophysical properties of the fluid, inclination of the substrate and contact angle hysteresis. Fluids with higher surface tension show a larger critical radius. Reduction in contact angle hysteresis reduces the critical radius of the droplet at fall-off for a given angle of inclination.

Acknowledgment

The authors are grateful to the Board of Research in Nuclear Sciences (BRNS), Department of Atomic Energy, Government of India for providing the financial assistance to carry out this research work. Help provided by Dr. Animangsu Ghatak in coating glass substrates is acknowledged.

Nomenclature

A = area of cross section (m^2)
a = acceleration of the moving droplet (m^2/s)
F = force (N)
h = latent heat of vaporization of the liquid (kJ/kg)
k = thermal conductivity (W/m K)
L = length (m)
M = molecular weight of the condensing liquid (kg/kmol)
q = surface heat flux (W/m^2)
R = universal gas coefficient (J/kmol K)
r = radius of droplet (m)
T = temperature (K)
ΔT = temperature drop (K)
Δt = time step (s)
U = velocity of the moving droplet (m/s)
V = volume of the drop (m^3)

Greek Symbols

α = inclination angle (deg)
η = dynamic viscosity (Pa s)
λ = wavelength of light (m)
ν = specific volume at the saturation temperature (m^3/kg)
ϕ = azimuthal angle (deg)
ρ = density (kg/m^3)
σ = surface tension of liquid (N/m)
$\hat{\sigma}$ = accommodation coefficient
τ = shear stress (N/m^2)
θ = contact angle (deg)

Subscripts

adv = advancing
avg = average

Downloaded 08 Nov 2010 to 202.3.77.11. Redistribution subject to ASME license or copyright; see http://www.asme.org/terms/Terms_Use.cfm

b = base
c = condensate
cond = conduction
crit = critical
curr = current
curv = curvature
d = droplet
g = gravity
int = interfacial heat and mass transfer
l = liquid
lv = liquid-vapor interface
max = maximum
min = minimum
prev = previous
r = retention
rcd = receding
sat = saturation
sl = solid-liquid interface
s = shear
sc = spherical cap
t = total
v = vapor
w = wall
$\parallel$ = parallel to the substrate
$\perp$ = perpendicular to the substrate

References

[1] Rose, J. W., 2002, "Dropwise Condensation Theory and Experiments: A Review," Proc. Inst. Mech. Eng., Part A, **216**, pp. 115–128.
[2] Leipertz, A., and Fröba, A. P., 2006, "Improvement of Condensation Heat Transfer by Surface Modification," *Proceedings of the Seventh ASME, Heat and Mass Transfer Conference*, IIT Guwahati, India, K7, pp. k85–k99.
[3] Carey, V. P., 1992, *Liquid-Vapor Phase-Change Phenomena*, Hemisphere, New York, pp. 342–351.
[4] Marto, P. J., Looney, D. J., and Rose, J. W., 1986, "Evaluation of Organic Coating for the Promotion of Dropwise Condensation of Steam," Int. J. Heat Mass Transfer, **29**, pp. 1109–1117.
[5] Zhao, Q., Zhang, D. C., Lin, J. F., and Wang, G. M., 1996, "Dropwise Condensation on L-B Film Surface," Chem. Eng. Process., **35**, pp. 473–477.
[6] Vemuri, S., Kim, K. J., Wood, B. D., Govindaraju, S., and Bell, T. W., 2006, "Long Term Testing for Dropwise Condensation Using Self-Assembled Monolayer Coating of N-Octadecyl Mercaptan," Appl. Therm. Eng., **26**, pp. 421–429.
[7] Rausch, M. H., Fröba, A. P., and Leipertz, A., 2008, "Dropwise Condensation Heat Transfer on Ion Implanted Aluminum Surfaces," Int. J. Heat Mass Transfer, **51**, pp. 1061–1070.
[8] Ma, X.-H., and Wang, B.-X., 1999, "Life Time Test of Dropwise Condensation on Polymer-Coated Surfaces," Heat Transfer Asian Res., **28**(7), pp. 551–558.
[9] Majumdar, A., and Mezic, I., 1999, "Instability of Ultra-Thin Water Film and the Mechanism of Droplet Formation on Hydrophobic Surfaces," ASME Trans. J. Heat Transfer, **121**, pp. 964–970.
[10] Bertier, J., 2008, *Microdrops and Digital Micro-Fluidics*, William Andrew, Norwich, NY, pp. 130–135.
[11] Sikarwar, B. S., Muralidhar, K., and Khandekar, S., 2010, "Flow and Thermal Fields in a Pendant Droplet Moving on Lyophobic Surface," 14th International Heat Transfer Conference, Washington, D.C., Paper No. IHTC14-22520.
[12] Leach, R. N., Stevens, F., Langford, S. C., and Dickinson, J. T., 2006, "Experiments and Simulations of Nucleate and Growth of Water Drops in a Cooling System," Langmuir, **22**, pp. 8864–8872.
[13] McCormick, J. L., and Baer, E., 1963, "On the Mechanism of Heat Transfer in Dropwise Condensation," J. Colloid Sci., **18**, pp. 208–216.
[14] Bansal, G. D., Khandekar, S., and Muralidhar, K., 2009, "Measurement of Heat Transfer During Dropwise Condensation of Water on Polyethylene," Nanoscale Microscale Thermophys. Eng., **13**, pp. 184–201.
[15] Tartarini, P., Lorenzini, G., and Randi, M. R., 1999, "Experimental Study of Water Droplet on Hot, Non-Porous Surfaces," Heat Mass Transfer, **34**(6), pp. 437–447.
[16] Briscoe, B. J., and Galvin, K. P., 1991, "The Sliding of Sessile and Pendent Droplets the Critical Condition," J. Colloid Interface Sci., **52**, pp. 219–229.
[17] Lawal, A., and Brown, R. A., 1982, "The Stability of an Inclined Pendent Drop," J. Colloid Interface Sci., **89**, pp. 332–345.
[18] Glicksman, R. L., and Hunt, W. A., 1972, "Numerical Simulation of Dropwise Condensation," Int. J. Heat Mass Transfer, **15**, pp. 2251–2269.
[19] Wu, W. H., and Maa, J. R., 1976, "On the Heat Transfer in Dropwise Condensation," Chem. Eng. J., **12**, pp. 225–231.
[20] Maa, J. R., 1978, "Drop-Size Distribution and Heat Flux of Dropwise Condensation," Chem. Eng. J., **16**, pp. 171–176.
[21] Abu-Orabi, M., 1998, "Modeling of Heat Transfer in Dropwise Condensation," Int. J. Heat Mass Transfer, **41**, pp. 81–87.
[22] Rose, J. W., and Glicksman, L. R., 1973, "Dropwise Condensation—The Distribution of Drop Sizes," Int. J. Heat Mass Transfer, **16**, pp. 411–425.
[23] Gose, E., Mucciordi, A. N., and Baer, E., 1967, "Model for Dropwise Condensation on Randomly Distributed Sites," Int. J. Heat Mass Transfer, **10**, pp. 15–22.
[24] Burnside, B. M., and Hadi, H. A., 1999, "Digital Computer Simulation of Dropwise Condensation From Equilibrium Droplet to Detectable Size," Int. J. Heat Mass Transfer, **42**, pp. 3137–3146.
[25] Vemuri, S., and Kim, K. J., 2006, "An Experimental and Theoretical Study on the Concept of Dropwise Condensation," Int. J. Heat Mass Transfer, **49**, pp. 649–657.
[26] Eucken, A., 1937, "Energie Und Stoffaustausch an Grenzflächen," Naturwiss., **25**, pp. 209–218.
[27] Briscoe, B. J., and Galvin, K. P., 1991, "Growth With Coalescences During Condensation," Phys. Rev. A, **43**, pp. 1906–1917.
[28] Rose, J. W., 1976, "Further Aspects of Dropwise Condensation Theory," Int. J. Heat Mass Transfer, **19**, pp. 1363–1370.
[29] Mu, C., Pang, J., and Liu, T., 2008, "Effect of Surface Topography of Material on Nucleation Site Density of Dropwise Condensation," Chem. Eng. Sci., **63**, pp. 874–880.
[30] Narhe, R., Beysens, D., and Nikolayev, V. S., 2004, "Contact Line Dynamics in Drop Coalescence and Spreading," Langmuir, **20**, pp. 1213–1221.
[31] Wu, M., Cubaud, T., and Ho, C. M., 2004, "Scaling Law in a Liquid Drop Coalescence Driven by Surface Tension," Phys. Fluids, **16**(7), pp. L51–L54.
[32] Liao, Q., Zhu, X., Xing, S. M., and Wang, H., 2008, "Visualization Study on Coalescence Between Pair of Water Drops on Inclined Surfaces," Exp. Therm. Fluid Sci., **32**(8), pp. 1647–1654.
[33] Das, A. K., and Das, P. K., 2009, "Simulation of Drop Movement of an Inclined Surface Using Smoothed Particle Hydrodynamics," Langmuir, **25**, pp. 11459–11466.
[34] Sikarwar, B. S., Muralidhar, K., and Khandekar, S., 2010, "Flow and Heat Transfer in a Pendant Liquid Drop on an Inclined Plane," *Proceedings of the Ninth ASME Heat and Mass Transfer Conference*, IIT Mumbai, India, Paper No. 345, pp. 1322–1329.
[35] Grand, N. L., Daerr, A., and Limit, L., 2005, "Shape and Motion of Drops Sliding Down an Inclined Plane," J. Fluid Mech., **541**, pp. 253–315.
[36] Pierce, E., Carmona, F. J., and Amirfazli, A., 2008, "Understanding of Sliding and Contact Angles Results in Tilted Plate Experiments," Colloids Surf., A, **323**, pp. 73–82.
[37] ElSherbini, A. I., and Jacobi, A. M., 2004, "Liquid Drops on Vertical and Inclined Surfaces: I. An Experimental Study of Drop Geometry," J. Colloid Interface Sci., **273**, pp. 556–565.
[38] Dimitrakopoulos, P., and Higdon, J. J. L., 1999, "On the Gravitational Displacement of Three-Dimensional Fluid Droplets From Inclined Solid Surfaces," J. Fluid Mech., **395**, pp. 181–209.
[39] Korte, C. M., and Jacobi, A. M., 2001, "Condensate Retention Effects on the Performance of Plain-Fin and Tube Heat Exchangers: Retention Data and Modeling," ASME J. Heat Transfer, **123**, pp. 926–936.
[40] Dussan, E. B., V, and Chow, R. T., 1983, "On the Ability of Drops or Bubbles to Stick to Non-Horizontal Surfaces of Solids," J. Fluid Mech., **137**, pp. 1–29.
[41] Bouteau, M., Cantin, S., Benhabib, F., and Perrot, F., 2008, "Sliding Behavior of Liquid on Tilted Langmuir-Blodgett Surfaces," J. Colloid Interface Sci., **317**, pp. 247–254.
[42] ElSherbini, A. I., and Jacobi, A. M., 2004, "Liquid Drops on Vertical and Inclined Surfaces: II. A Method for Approximating Drop Shapes," J. Colloid Interface Sci., **273**, pp. 566–575.
[43] Extrand, C. W., and Kumara, Y., 1995, "Liquid Drop on an Inclined Plane: The Relation Between Contact Angles, Drop Shape and Retentive Forces," J. Colloid Interface Sci., **170**, pp. 515–521.
[44] Sakai, M., Hashimoto, A., Yoshida, N., Suzuki, S., Kameshima, Y., and Nakajima, A., 2006, "Direct Observation of Internal Fluidity in a Water Droplet During Sliding on Hydrophobic Surfaces," Langmuir, **22**, pp. 4906–4909.
[45] Kim, H. Y., Lee, H., and Kang, B. H., 2002, "Sliding of Drops Down an Inclined Solid Surface," J. Colloid Interface Sci., **247**, pp. 372–380.
[46] Sadhal, S. S., 1997, *Transport Phenomena With Drops and Bubbles* (Mechanical Engineering Series), Springer, New York, pp. 218–230.
[47] Koch, G., Kraft, K., and Leipertz, A., 1998, "Parameter Study on the Performance of Dropwise Condensation," Int. J. Therm. Sci., **37**, pp. 539–548.

Downloaded 08 Nov 2010 to 202.3.77.11. Redistribution subject to ASME license or copyright; see http://www.asme.org/terms/Terms_Use.cfm